

Simulation-based planning of Motion Sequences for Automated Procedure Optimization in Multi-Robot Assembly Cells

Loris Schneider , Marc Ungen , Elias Huber , Jan-Felix Klein 

This work has been submitted to the IEEE for possible publication. Copyright may be transferred without notice, after which this version may no longer be accessible.

Abstract—Reconfigurable multi-robot cells offer a promising approach to meet fluctuating assembly demands. However, the recurrent planning of their configurations introduces new challenges, particularly in generating optimized, coordinated multi-robot motion sequences that minimize the assembly duration. This work presents a simulation-based method for generating such optimized sequences. The approach separates assembly steps into task-related core operations and connecting traverse operations. While core operations are constrained and pre-determined, traverse operations offer substantial optimization potential. Scheduling the core operations is formulated as an optimization problem, requiring feasible traverse operations to be integrated using a decomposition-based motion planning strategy. Several solution techniques are explored, including a sampling heuristic, tree-based search and gradient-free optimization. For motion planning, a decomposition method is proposed that identifies specific areas in the schedule, which can be solved independently with modified centralized path planning algorithms. The proposed method generates efficient and collision-free multi-robot assembly procedures that outperform a baseline relying on decentralized, robot-individual motion planning. Its effectiveness is demonstrated through simulation experiments.

Note to Practitioners— In practice, robotic motions in multi-robot assembly cells are often handcrafted for specific tasks, requiring significant effort and lacking scalability. This paper presents a novel method for optimizing robotic motion sequences and their execution schedules with the goal of minimizing the assembly duration. Existing approaches for combined task and motion planning often rely on high-level heuristics, impose restrictive constraints on planning, or demand excessive computational resources. . The proposed method separates task-related motions, which perform essential transformations on the assembly product, from connecting traverse motions. Task-related motions are pre-planned and treated as fixed building blocks of the schedule, enabling broad applicability across diverse assembly tasks. The method minimizes total assembly time by optimizing the execution schedule of these task-related motions, while treating the existence of feasible traverse motions as a constraint. This constraint is evaluated through a centralized, multi-modal, multi-robot motion planning approach that uncovers optimization potential typically missed by decentralized methods. We examine various optimization strategies, including sampling-based and gradient-free techniques. Simulation experiments with two to four robots on an assembly task demonstrate significant

reductions in assembly duration compared to prior methods, with acceptable computational effort. However, the approach currently scales exponentially with the number of robots and does not yet generate full actuator-level motion profiles. Future work will address these limitations to enable deployment on real-world robotic systems.

I. INTRODUCTION

FLUCTUATIONS in resource availability and growing demand for customized products are driving the development of adaptive assembly systems. A key feature of such systems is their ability to adjust functionality within a fixed structural configuration [1]. Multi-robot cells present a promising solution for adaptive assembly systems by employing flexible, general-purpose robotic manipulators. The use of multiple robots allows parallel execution of tasks, thereby offering potential to reduce the overall assembly duration. In order to realize this potential, optimization over the structural and procedural configuration of a multi-robot cell is required. The structural configuration describes the current set of machine modules and robotic manipulators and their placement and arrangement in the cell's workspace. The procedural configuration describes the implemented procedural flow that, together with the structural configuration, results in the assembly of a specific product. Specifically, the procedural configuration consists of timed low-level control signals for the robots, tools, and machines involved. Finding an optimized procedural configuration involves solving multiple nested optimization problems in different domains, e.g. task planning and scheduling and robotic motion planning.

A. Procedural configuration taxonomy

To systematically analyze the generation of optimized procedural configurations, we introduce a taxonomy that provides a unified, high-level framework for characterizing the various aspects inherent to procedural configurations of multi-robot assembly cells.

Assembly task: The assembly task represents the overall objective to be accomplished by the multi-robot cell. It is solely defined by the product requirements and is independent of any particular structural and procedural configuration. To model this task, an assembly precedence graph is used which outlines the required assembly steps and establishes the precedence constraints among them. Figure 1a shows an example for such a graph for a representative assembly task.

Assembly step: An assembly step is a node in the assembly precedence graph and directly contributes to the completion of the product. Figure 1b demonstrates how the exemplary assembly precedence graph can be translated into a high-level

Loris Schneider, Elias Huber and Jan-Felix Klein are with the Institute for Material Handling and Logistics (IFL), Karlsruhe Institute of Technology, 76131, Germany. loris.schneider@kit.edu.

Marc Ungen and Elias Huber are researchers at Bosch Corporate Research, Robert Bosch GmbH, 71272 Renningen, Germany. marc.ungen@de.bosch.com

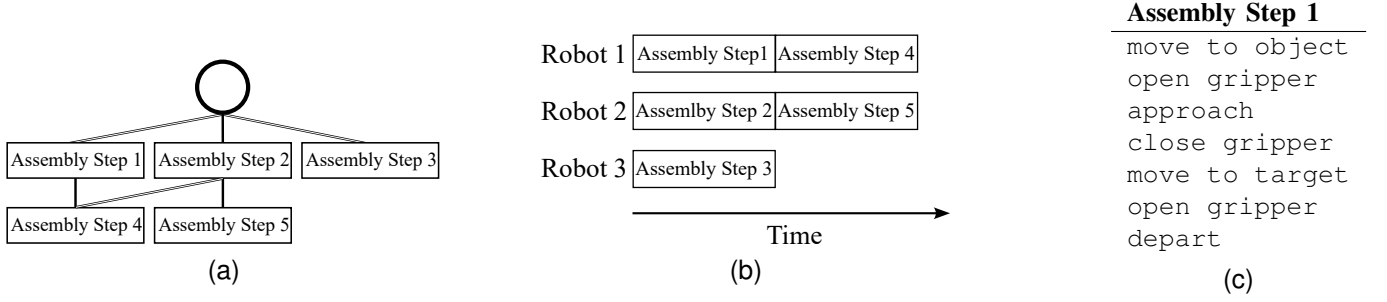


Fig. 1. Assembly precedence graph with assembly steps (a), assignment of assembly steps to robots (b) and decomposition of an assembly step into actions (c).

execution schedule by assigning assembly steps to individual robots.

Action: Robots and machines execute assembly steps by performing one or more actions. These actions represent low-level execution steps that not only depend on the assembly step but also on the specific structural and procedural configuration of the system. The complete set of actions, along with their corresponding execution schedule, defines the procedural configuration. Actions may encompass a wide range of activities ranging from end-effector control (e.g., opening or closing a gripper) to motions (e.g., moving between joint configurations). Figure 1c illustrates how a single assembly step, such as picking up an object with a gripper and placing it at a target location, can be decomposed into a sequence of low-level actions. Depending on the system design and granularity of control, both finer or coarser decompositions are possible.

B. Problem description

In the context of generating optimized procedural configurations, this work addresses the problem of determining and scheduling efficient motion actions for a given structural configuration and a predefined assignment of assembly steps to robots. The outcome is a set of precise motion instructions specifying how and when each robot should move in order to minimize the total assembly duration while ensuring completion of the assembly task. Other types of actions are assumed to be predefined and are not within the scope of this work.

Determining and scheduling optimized motion actions for multi-robot assembly cells presents several challenges: Robots operating within a shared workspace become dynamic obstacles to one another during simultaneous motion execution. As the number of robots is increased, the combined C -spaces grows with the total number of joints, leading to an exponential rise in computational effort, unless strategies are applied to reduce C -space dimensionality. Furthermore, when robots pick up tools or parts, their structure changes, which affects how their movements translate into possible collisions. As a result, the mapping between the physical workspace and the collision-free C -space becomes unstable and difficult to predict.

This work presents a method for identifying and scheduling of optimized motion actions for multi-robot assembly cells,

effectively addressing the challenges outlined above.

The paper is organized as follows: Section II reviews and summarizes relevant related work. Section III introduces the overall approach, which is based on decomposing the problem into scheduling the task-related core motions and interpolating valid traverse motions. Section IV further investigates the scheduling problem and presents various solution strategies. In Section V a novel motion planning strategy is described that integrates valid traverse motions into a given schedule of core motions. Section VI evaluates the proposed scheduling and motion planning methods in simulated multi-robot cells with varying structural configurations. Section VII discusses the results and outlines the limitations of the proposed approach and summarizes the key contributions.

II. RELATED RESEARCH

This section illustrates related fields of research and selected related work.

A. Related fields of research

1) *Motion planning:* Robotic motion planning focuses on computing feasible, collision-free motions for one or more robots in the presence of obstacles. A central subproblem is path planning, often addressed using sample-based algorithms. To handle differential constraints, motion planning is typically decoupled. First a path is determined, then, joint velocities and accelerations are computed along it - a process known as parametrization [2]. For instance, Pham and Pham proposed a parametrization algorithm to obtain execution time-optimal joint acceleration and velocity trajectories [3].

Dynamic obstacles with known trajectories can be handled by extending the configuration space C with time T , resulting in a space-time state space $X = C \times T$. Sintov and Shapiro [4] and Grothe et al. [5] presented adaptations of state-of-the-art path planning algorithms to handle space-time state spaces. In multi-robot systems, the joint C -space dimensionality increases significantly which complicates the motion planning. To manage this, centralized methods plan in the combined C -Space using prioritization or dimensionality-abstraction to reduce complexity [6]–[8], while decentralized approaches simplify the problem by planning for each robot individually and sequentially [9]. While centralized approaches focus on

completeness, decentralized approaches aim for efficiency in motion planning.

2) *Multi-modal motion planning*: Multi-modal motion planning addresses scenarios where the robot's kinematic chain changes. This introduces discrete kinematic states and related constraints which are expressed as kinematic graphs $G = (V, E)$. Vertices V denote rigid bodies and joints, while edges E represent attachments including relative transformations.

These graphs model how connections in the kinematic chain are formed or broken, with each discrete state defining a specific mode that affects link structure and collision geometry. Multi-modal motion planning is based on building multiple data structures that represent a robot's C -space for each individual mode and connecting them at specific mode switches. Searching over these structures enables motion planning across different modes [10], [11].

3) *Task and motion planning*: Task and motion planning (TAMP) integrates the aspects of motion planning or multi-modal motion planning with classical task planning. Classical planning operates in a discrete state space S , typically expressed in first-order logics, with the aim to find sequences that transform an initial state to a desired goal state.

TAMP therefore introduces hybrid problems characterized by mixed discrete-continuous state spaces with complex constraints, which are referred to as hybrid constraint satisfaction problems (H-CSPs). As outlined by Garret et al. [12], solution strategies to H-CSPs fall into three categories: sequencing-first, satisfaction-first and hybrid approaches:

- Sequencing-first approaches generate a high-level task plan (plan skeleton) and attempt to solve motion planning for each step. If motion planning fails, a new skeleton is generated through backtracking.
- Satisfaction-first methods precompute feasible motions and mode transitions, restricting task planning to those. Failures trigger the generations of more motions and mode switches.
- Hybrid approaches combine aspects from both sequencing-first and satisfaction-first approaches.

B. Related work

Hartmann et al. present a multi-robot TAMP approach for long-horizon construction tasks using mobile manipulators [13]. Assembly steps are iteratively assigned and executed with locally optimized, asynchronous motions. The methods scales linearly with the number of robots.

Chen et al. aim to minimize the assembly duration using annotated, robot-specific roadmaps containing object grasps and connecting motions [14]. The individual roadmaps are compared, and joint configurations resulting in possible collisions between the robots are identified and annotated in the roadmaps. The global procedure is then built by using the information in the annotated roadmaps. This way, different grasps and motions can be considered to minimize the assembly duration. However, annotating the roadmaps with collision information is time consuming, limiting its applicability for adaptive systems.

Ungen et al. present an approach to generate assignments of assembly steps to robots and sequences of assembly steps to optimize the duration of assembly tasks in reconfigurable multi-robot assembly cells [15]. The approach efficiently finds an optimized temporal arrangement of motions using pre-planned motions for each individual robot. The approach does not exploit coordinated multi-robot execution, leaving room for further reduction in assembly durations.

Zhang et al. addresses multi-robot pick-and-place tasks with a sequencing-first TAMP approach [16]. Plan skeletons aiming for short assembly durations are generated and partially filled, then refined using a Monte Carlo Tree Search (MCTS) over a tree of skeletons. The search favors skeletons with fewer object movements, indirectly minimizing assembly duration.

Mateu-Gomez et al. propose a multi-robot TAMP approach for pick-and-place tasks that directly incorporates motion planning to optimize the task duration [17]. The workspace is discretized into a grid, with each point assigned feasible joint configurations for each robot and annotated with collision information. Robots are modeled as points moving between neighboring grid cells, allowing the problem to be formulated as a Markov Decision Process. However, optimization is limited to the predefined joint configurations at each grid point.

III. GENERAL APPROACH

Building on the work of [15], the approach proposed in this work assumes a well-defined assembly task described by a set of assembly steps and an associated assembly precedence graph. A multi-robot cell with a fixed structural configuration is provided, where each robot is assigned a unique subset of assembly steps. The assembly process, the structural configuration and the assembly step assignments are assumed to satisfy the following conditions:

- 1) All required components and tools are available, with known initial and goal locations.
- 2) Each assembly step is associated with the specific components and tools needed for its execution.
- 3) The assigned robot can reach all components, tools and goal locations relevant to its operations. Handovers are not required.
- 4) Each robot has a defined escape configuration in which it does not collide with other robots or objects.

A. Problem decomposition

As shown in Figure 1c, each assembly step can be decomposed into a sequence of actions. Those actions can be combined into groups which we call operations. We generally distinguish between two categories of operations, **core operations** and **traverse operations**.

Core operations are productive steps that characterize the corresponding operation, e.g., a screwing process. Traverse operations describe the motion of a robot from its current joint configuration to the start joint configuration of the following core operation and consist of only one motion action. Thus, each assembly step contains a series of alternating traverse and core operations. Table I shows how different actions may be assigned to traverse and core operations.

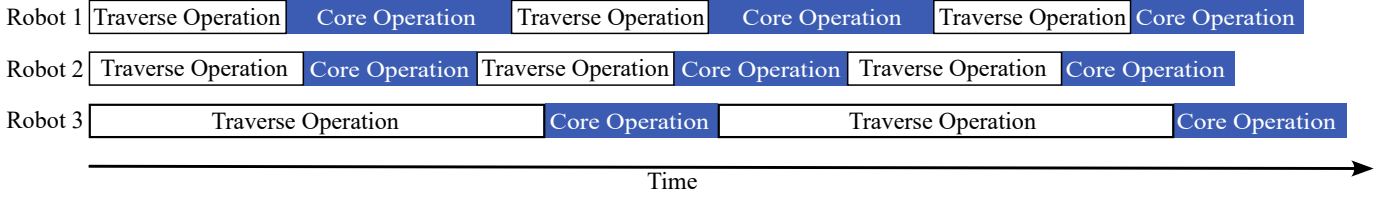


Fig. 2. Example of a schedule of preplanned core operations with interpolated traverse operations.

TABLE I
ASSIGNMENT OF ACTIONS TO TRAVERSE AND CORE OPERATIONS.

Action	Operation
move to object	Traverse Operation
open gripper	Core Operation
approach	
close gripper	
move to target	Traverse Operation
open gripper	Core Operation
depart	

The first step of the proposed approach is to find suitable motions for each robot's core operations. These involve critical and sensitive manipulations and may be subject to various constraints, e.g., with respect to end-effector poses or applied forces. Therefore, core operations are preplanned and represented as time-parametrized trajectories of joint configurations, with fixed durations and step intervals.

In this work, constraints on core motions are encoded as end-effector waypoints. Corresponding joint trajectories are computed using an inverse kinematic solver and a time-optimal path parametrization algorithm [3], ensuring smooth execution with zero velocity at start and end.

Once defined, core operations act as fixed building blocks. With fixed core operations, the problem reduces to two inter-related subproblems:

- 1) Scheduling: Determine suitable start times for each core operation.
- 2) Motion Planning: Find valid traverse motions between core operations.

The scheduling problem is investigated in Section IV, and the motion planning problem in Section V.

Due to their interdependency, the proposed approach adopts a sequencing-first strategy: A schedule for core operations is generated first, see Figure 2, treating core operations as fixed-duration units. The white segments represent traverse operations, for which valid, collision-free motions are interpolated within the time windows defined by the schedule. The resulting traverse motions are then fed back into the scheduling process to iteratively improve the overall solution.

IV. SCHEDULING

Given all N core operations $O^{\text{core}} = [o_1^{\text{core}}, o_2^{\text{core}}, \dots, o_N^{\text{core}}]$, a schedule can be represented as an N -dimensional vector θ , where each element specifies the start time of a core

operations. This yields the following optimization problem:

$$\min_{\theta} d(\theta) \quad (1)$$

$$\text{s.t. } c(\theta) = 0 \quad (2)$$

$$p(\theta) \geq 0 \quad (3)$$

$$m(\theta) \geq 0 \quad (4)$$

Here, $d(\theta)$ denotes the assembly duration resulting from a schedule θ . The constraints are defined as follows:

- Constraint (2) ensures that core operations do not lead to collisions between robots or between robots and objects.
- Constraint (3) enforces the precedence relations among core operations.
- Constraint (4) guarantees that sufficient time is allocated between consecutive core operations on the same robot to allow for collision-free traverse motions, subject to each robot's joint velocity and acceleration limits.

The evaluation of (4) requires solving the motion planning problem and is addressed in Section V. Since solving this constraint exactly is computationally expensive, it is initially approximated using a lower bound. To compute this approximation, traverse motions are preplanned in a decentralized manner using path planning algorithms and then shortened using a shortcutting technique. Afterwards a trajectory is generated using a time-optimal path parametrization algorithm [3]. This yields an estimate of the minimum required duration for each traverse operation. During initial scheduling, instead of verifying the existence of a valid full motion plan between two core operations, the schedule must simply allow enough time to satisfy these estimated durations. This relaxed constraint is expressed as:

$$m'(\theta) \geq 0 \quad (5)$$

Using this approximation and the known durations of core operations, a lower bound d_{\min} on the total assembly duration can be calculated. This bound respects the precedence constraints in (3), but ignores potential collisions of traverse motions.

A. Sampling heuristic

To support the identification of a feasible schedule θ that satisfies constraints (2), (3) and (5), while also yielding a short assembly duration, two additional relaxations are introduced:

- The time is discretized into fixed-length time steps.
- A maximum assembly duration d_{\max} is specified. This may be defined as a fixed multiple of the lower bound d_{\min} , or adjusted as a tunable parameter to influence the scheduling outcome.

These relaxations enable the construction of a sample-based heuristic for generating candidate schedules. The pseudocode for the proposed scheduling method is presented in Algorithm 1. The algorithm proceeds as follows: At each step, it identifies core operations that are eligible for scheduling. A core operation is considered *primed* if it has no predecessors or if all of its predecessors have already been scheduled. From the set of primed core operations, one is randomly selected for scheduling. For the selected operation, a feasible scheduling interval is computed. This interval is bounded as follows:

- The earliest feasible start time corresponds to the latest end time among all its preceding core operations and the corresponding traverse operations.
- The latest permissible start time ensures that the core operation, along with its subsequent traverse operations and any required successor operations, can still be scheduled without exceeding d_{\max} .

Algorithm 1 Scheduling by sampling heuristic

```

1:  $O_{\text{closed}}^{\text{core}} \leftarrow \emptyset, O_{\text{open}}^{\text{core}} \leftarrow O^{\text{core}}$ 
2: while not  $O_{\text{open}}^{\text{core}} = \emptyset$  do
3:    $O_{\text{primed}}^{\text{core}} \leftarrow \text{getPrimedCoreOperations}(O_{\text{open}}^{\text{core}}, O_{\text{closed}}^{\text{core}})$ 
4:    $o^{\text{core}} \leftarrow \text{randomChoice}(O_{\text{primed}}^{\text{core}})$ 
5:    $I \leftarrow \text{getSchedulingInterval}(o^{\text{core}}, O_{\text{open}}^{\text{core}}, O_{\text{closed}}^{\text{core}})$ 
6:   if  $I = \emptyset$  then
7:      $\text{resetScheduledCoreOperations}(O_{\text{closed}}^{\text{core}})$ 
8:      $O_{\text{closed}}^{\text{core}} \leftarrow \emptyset, O_{\text{open}}^{\text{core}} \leftarrow O^{\text{core}}$ 
9:     go to line 2
10:  end if
11:   $P \leftarrow \text{getSelectionProbabilities}(I)$ 
12:   $s \leftarrow \text{chooseStartTimeStep}(I, P)$ 
13:   $\text{assignStartTimeStep}(o^{\text{core}}, s)$ 
14:  while  $\text{collision}(o^{\text{core}}, O_{\text{closed}}^{\text{core}})$  is true do
15:     $I.\text{pop}(s)$ 
16:    if  $I = \emptyset$  then
17:       $\text{resetScheduledCoreOperations}(O_{\text{closed}}^{\text{core}})$ 
18:       $O_{\text{closed}}^{\text{core}} \leftarrow \emptyset, O_{\text{open}}^{\text{core}} \leftarrow O^{\text{core}}$ 
19:      go to line 2
20:    end if
21:     $P \leftarrow \text{getSelectionProbabilities}(I)$ 
22:     $s \leftarrow \text{chooseStartTimeStep}(I, P)$ 
23:     $\text{assignStartTimeStep}(o^{\text{core}}, s)$ 
24:  end while
25:   $O_{\text{closed}}^{\text{core}}.\text{push}(o^{\text{core}}), O_{\text{open}}^{\text{core}}.\text{pop}(o^{\text{core}})$ 
26: end while

```

Next, selection probabilities are computed for each time step within the scheduling interval. The chosen probability distribution over the interval serves as a tuning parameter that can be designed to bias the sampling toward promising regions. Based on the probabilities, a start time step is sampled and assigned to the selected core operation. The operation is then checked for collisions with previously scheduled core operations. If a collision is detected the assigned start time step is removed from the scheduling interval, the selection probabilities are updated accordingly, and a new time step is sampled. This process repeats until a collision-free assignment is found. If the scheduling interval becomes empty, the algorithm restarts

from scratch. In practice, this restart strategy was found to be more efficient than backtracking.

The presented sampling heuristic enables the generation of schedules that satisfy the constraints (2), (3) and (5). Minimization of the assembly duration is encouraged implicitly by biasing the sampling towards earlier time steps and through the enforcement of the global upper bound d_{\max} .

B. Gradient-free optimization

An alternative strategy is to reformulate the optimization problem to enable the use of gradient-free optimization techniques. This can be achieved by incorporating the strict collision constraint (2) as a penalty term within the objective function. Consequently, generated schedules are only required to satisfy constraints (3) and (5). The resulting optimization problem is defined as:

$$\begin{aligned}
 \min_{\theta} \quad & d(\theta) + \mu_1 c^2(\theta) + \mu_2 (\max\{0, d(\theta) - d_{\max}\})^2 \quad (6) \\
 \text{s.t.} \quad & p(\theta) \geq 0 \\
 & m'(\theta) \geq 0
 \end{aligned}$$

The second penalty term $(\max\{0, d(\theta) - d_{\max}\})^2$ discourages solutions that reduce collisions by excessively extending the overall schedule duration. The penalty weights μ_1 and μ_2 balance the relative importance of each term. To prevent convergence to local minima where marginal increases in assembly duration beyond d_{\max} lead to fewer collisions, it is advisable to set $\mu_2 \gg \mu_1$.

This work evaluates three gradient-free optimization methods: Simulated Annealing (SA) [18] with a statistical cooling strategy [19] as proposed in [20], Particle Swarm Optimization (PSO) [21], and an Evolutionary Algorithm (EA). These methods are adapted to satisfy the remaining constraints and can be initialized by generating random schedules within constraints (3) and (5). Alternatively, the sampling heuristic introduced in Section IV-A can be used for a penalty-free initialization.

Information from motion planning is fed back into the objective function as described in Section V-D. Detailed parameter settings for the employed optimization methods are provided in Section VI.

C. Decision tree

The scheduling problem can also be modeled as a decision tree. The core operations correspond to nodes in the decision tree, appearing in a predetermined scheduling order. The possible time steps within the operation's scheduling interval are represented as outgoing edges from that node. A complete schedule then corresponds to a path through the tree from the root to a leaf node. Terminal nodes can represent either valid schedules or invalid ones, such as those involving collisions or infeasible timing. This decision tree implicitly encodes all possible schedule configurations—both feasible and infeasible. By systematically exploring the tree, it is possible to search for a valid and efficient schedule. A well-established method for exploring such decision trees is Monte Carlo Tree Search (MCTS). MCTS is based on four main phases: Selection, Expansion, Simulation and Backpropagation.

During the selection phase, a common policy is to use the Upper Confidence Bounds Applied to Trees (UCT) rule proposed by [22], which selects the child node that maximizes the following expression for expanding the tree:

$$v_c + c\sqrt{\frac{\ln n_p}{n_c}}$$

Where v_c is the average value of the child node, n_p is the number of times the algorithm visited the parent node, n_c is the number of visits of the child node and c is a constant parameter.

Since MCTS is typically designed for problems where the objective is to maximize a scalar value between 0 and 1, the optimization objective function is adapted and normalized with the maximum possible result value to obtain the result value function:

$$r(\theta) = \begin{cases} \frac{\lambda_1 N_{\text{free}}}{d_{\text{max}} - d_{\text{min}} + \lambda_1 N}, & \text{if } c(\theta) \neq 0 \\ 0, & \text{if } d(\theta) > d_{\text{max}} \\ \frac{d_{\text{max}} - d(\theta) + \lambda_1 N}{d_{\text{max}} - d_{\text{min}} + \lambda_1 N}, & \text{else} \end{cases} \quad (7)$$

Here, N is the number of all core operations and N_{free} is the number of scheduled core operations that do not result in collisions. By including N_{free} , this result value function leads to higher result values if the number of core operations that are scheduled without collisions before reaching a terminal node increases. The weighting parameter λ_1 balances the influence of N_{free} against the assembly duration.

During simulation, MCTS can execute completely random, light playouts or use a more promising strategy during so-called heavy playouts. Here, the sampling heuristic described in Section IV-A can be used as a strategy for heavy playouts. In this case, instead of choosing a primed core operation for scheduling, the core operations are chosen according to the scheduling order.

MCTS is most commonly applied to decision trees of two-player games. Since this use case is different, a modified version of MCTS was developed. This version is expected to behave more greedily and is called MCTS-Greedy (MCTS-G). The adaptations to the classic MCTS are as follows:

- Each node holds the best result value of all its visits instead of the average.
- The explored tree is expanded not only by a single leaf child node but by the whole playout path.
- Selection does not necessarily stop at any leaf node. If a leaf node with at least one explored child node is encountered, selection ends only with a certain probability. Otherwise, selection continues among the explored child nodes.

The idea is to identify the best encountered paths and explore the decision tree around those. This is illustrated in Figure 3 which visualizes how the explored decision tree grows. The initial explored decision tree in Figure 3a contains the best path encountered which is marked with green nodes. During selection in Figure 3b, a promising path is followed as indicated by the yellow edges. Since UCT is applied during selection, this path is not necessarily the best encountered path. At a random node with unexplored edges, exploration starts

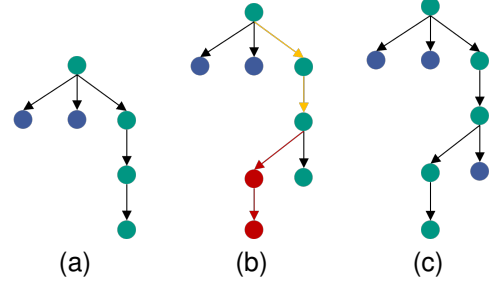


Fig. 3. Exploration of the decision tree by MCTS-G.

by diverting from the path which is marked with red edges and nodes. After reaching a terminal node and calculating the result value, the new explored path is added to the explored tree in Figure 3c. In this case, the newly added path could improve on the best encountered path and is marked as the new best encountered path.

V. MOTION PLANNING

All described scheduling methods in Section IV rely on the relaxed motion planning constraint (5). However, to obtain a valid schedule, the stricter constraint (4) must ultimately be satisfied. This section outlines how (4) is evaluated for a promising schedule and how results are fed back into the scheduling process. Algorithm 2 shows the main steps of the presented multi-robot motion planning method.

Algorithm 2 High-level flow of the motion planning

```

1:  $K \leftarrow \text{identifyProblemAreas}(\theta)$ 
2:  $K' \leftarrow \emptyset$ 
3: for  $k \in K$  do
4:    $R \leftarrow \text{initializeCrossSectionalRoadmap}(k)$ 
5:    $K'.\text{push}(k, R)$ 
6: end for
7: for  $k, R \in K'$  do
8:    $G \leftarrow \text{getGuidePath}(R)$ 
9:   while  $G = \emptyset$  do
10:     $R \leftarrow \text{extendCrossSectionalRoadmap}(k, R)$ 
11:     $G \leftarrow \text{getGuidePath}(R)$ 
12:   end while
13:    $S \leftarrow \emptyset$ 
14:   for  $p \in G$  do
15:     $s \leftarrow \text{solveMotionPlanningProblem}(p)$ 
16:    if not  $s$  then
17:       $R \leftarrow \text{removeEdge}(R, s)$ 
18:      go to line 8
19:    end if
20:     $S.\text{push}(s)$ 
21:   end for
22: end for

```

A. Identification of Problem Areas

The algorithm starts by identifying so-called *problem areas*. Figure 4 illustrates an exemplary schedule involving three

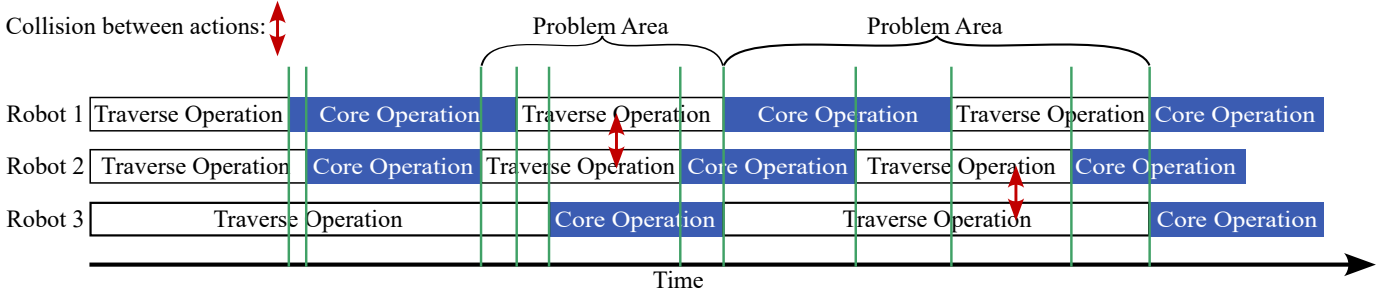


Fig. 4. Identification of problem areas in a schedule based on collisions of traverse operations.

robots. The schedule is initially segmented into sections by identifying all time steps where a core operation starts or ends (green vertical lines).

Since mode switches solely occur during a core operation, each section is characterized by traverse operations of constant modes. Sections containing only core operations are excluded from further motion planning since they have already been verified to be collision-free during scheduling.

The initially planned motions are assigned to the traverse operations, resulting in a complete tentative assembly procedure. This procedure is then checked for collisions. If a collision is encountered, the involved traverse operations are collected and the corresponding sections are grouped to form a *problem area* which can be solved independently. All sections that are not part of a *problem area* do not require further attention and the initially planned motions can be applied safely.

In the exemplary schedule in Figure 4, two collisions during traverse operation motions were encountered (red double arrows) resulting in two problem areas spanning multiple sections and traverse operations.

B. Creating Cross-Sectional Roadmaps

To resolve each identified problem area, an abstract *cross-sectional roadmap* is constructed that spans across all sections encompassed by that problem area. At each section boundary, configurations are sampled from the combined C -space of all robots performing a traverse operations at this particular time step. Robots executing core operation are considered to be in a known and fixed joint configuration and are treated as static obstacles. The sampled configurations are checked for collisions and collision-free configurations are retained for further use.

To ensure that only reachable configurations are sampled, the strategy includes calculating reachable joint angle intervals for each individual robot. This is done based on:

- The last fixed configuration of each robot,
- the time elapsed since that configuration,
- each robot's velocity and acceleration limits.

This approach constraints the sampling space to feasible regions of the C -space.

An attempt is made to connect all collision-free configurations at each section boundary to those at the subsequent boundary. A connection is valid if the motion between the configurations is feasible, given their temporal spacing, their spatial distance

in C -space, and the velocity and acceleration limits of the respective robots. If no valid connection can be established, new samples are generated on each border until a connection is found or an iteration limit is reached.

The resulting configurations and their connections form a directed graph, a cross-sectional roadmap, see Figure 5. Each edge is assigned a weight corresponding to the distance in C -space. Every roadmap starts at a single configuration and ends with a single configuration. Once the roadmap is constructed, Dijkstra's algorithm [23] is used to compute the shortest path, which we refer to as the *guide path*, highlighted in yellow in Figure 5. During the roadmap initialization, new configurations are sampled until a complete guide path is available.

C. Motion Planning along guide paths

Each edge in the guide path corresponds to an individual motion planning problem defined by a start and goal configuration. Robots performing core operations during each problem are viewed as dynamic obstacles with known joint configurations and collision geometries at every time step. Each motion planning problem is expressed in the combined X -space of the robots executing traverse operations within the corresponding section.

To solve these individual problems, the Probabilistic Roadmap (PRM) algorithm [24] and the RRT-connect algorithm [25] are employed. The time dimension of the X -space requires certain modifications: When connecting sampled configurations in time, the robot's acceleration and velocity limits have to be considered and connections that move backwards in time cannot be permitted.

The solution of a motion planning problem is extended by the known configurations of the robots performing core operations at each time point to form a collision-free solution path through the combined X -space of all robots in a section.

If an individual motion planning problem cannot be solved, the corresponding edge is removed from the cross-sectional roadmap. A new guide path is computed. If no valid guide path exists, the roadmap is incrementally extended with additional samples until a feasible guide path is found.

Using the guide path, the solutions of each problem are connected to form a collision-free trajectory through the entire problem area in the combined X -space of all robots.

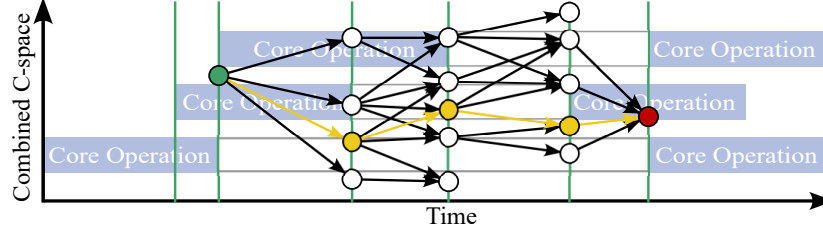


Fig. 5. A cross-sectional roadmap with a guide path.

D. Feeding back motion planning results

Some problem areas may not contain a solvable guide path. This can occur either because the cross-sectional roadmap contains no valid guide path, or because none of the candidate paths can be successfully solved.

The presented motion planning approach does not inherently detect unsolvable cases and may continue searching indefinitely. To avoid this, a termination criteria is introduced. When constructing the initial cross-sectional roadmap, the number of sampling attempts without finding a collision-free sample at each section border is limited. This sampling limit L grows exponentially with the number of involved robots n_r , according to $L = L_0^{n_r}$ where L_0 is a constant. In addition, each single motion planning problem is subject to a fixed solving time limit.

When repeatedly trying to solve proposed guide paths for a problem area, the algorithm is additionally required to find a guide path that contains more solved sections than the previous guide path with the most solved sections within a certain time. This way, motion planning continues as long as solutions to motion planning problems in new sections of a problem area are found but does not become trapped in unsolvable problems. Two distinct failure cases are identified based on these criteria:

- 1) Reaching the sampling limit at a section border during initial roadmap construction.
- 2) Exceeding the time limit when attempting to solve proposed guide paths.

For both failure cases, a measure of the *magnitude of failure* is defined. In the first case, the time point of the section border where the sample limit L was surpassed is identified. In the second failure case, the latest time point of the goal configuration of all solved sections is tracked.

In both cases, the magnitude of failure can be expressed by counting the number of traverse operations that end before the respective time point. This number is denoted with A_R for the first case and A_P for the second case.

These quantities are integrated into the gradient-free optimization methods. The objective function in Equation (6) is extended with a penalty term:

$$-\mu_3 A_P - \mu_4 A_R$$

Here, μ_3 and μ_4 are weights balancing the influence of A_R and A_P .

Similarly, the result value function (7) of the MCTS-based

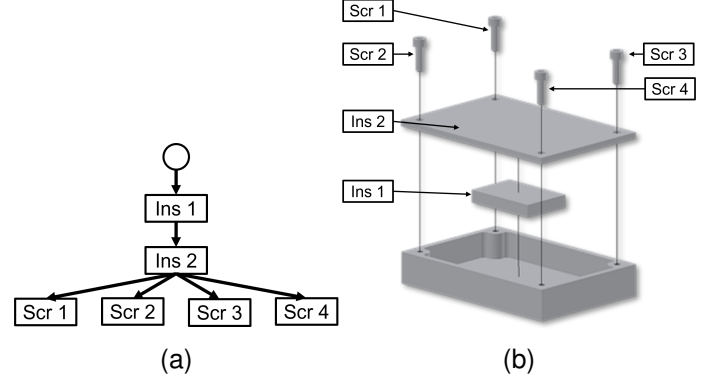


Fig. 6. Assembly precedence graph (a) and assembly components (b).

methods is adapted by extending the non-zero cases to:

$$\frac{\lambda_1 N_{\text{free}}}{d_{\text{max}} - d_{\text{min}} + \lambda_1 N + \lambda_2 N + \lambda_3 N}$$

if $c(\theta) \neq 0$ and

$$\frac{d_{\text{max}} - d(\theta) + \lambda_1 N + \lambda_2 A_P + \lambda_3 A_R}{d_{\text{max}} - d_{\text{min}} + \lambda_1 N + \lambda_2 N + \lambda_3 N}$$

in the default case with the weights λ_2 and λ_3 .

Finally, successfully solved guide paths are post-processed to improve path quality. This includes applying short-cutting, corner-cutting [26], partial short-cutting [27] and moving-average smoothing.

VI. EVALUATION

To evaluate the presented methods, an experimental setup and an assembly task were designed:

The assembly task consists of assembling seven components to a small box. Figure 6b shows the components and their respective assembly steps as well as the assembly precedence graph. The robots can use suction grippers to place a small object inside the box and to place the lid on the box, as well as screwdrivers to fix the lid with four screws. Precedence constraints are expressed in the assembly precedence graph in Figure 6a. This assembly task is executed using structural configurations with two, three, and four robots where each robot has an individual tool holder and individual tools. The structural configurations with two, three, and four robots are shown in Figure 7.

The experiments were conducted in a simulation environment,

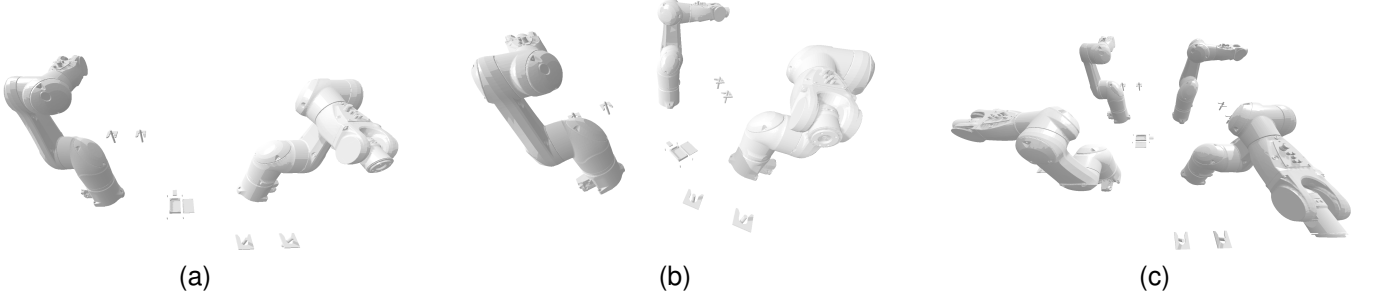


Fig. 7. Structural configurations with two (a), three (b) and four (c) robots.

using the Pybullet physics engine [28] for visualization, rigid body simulation and collision checking. For path planning, the implementations of PRM and RRT-connect from the Open Motion Planning Library (OMPL) [29] were used and adapted using OMPL's own Python API. All experiments ran inside virtual machines on a system with two 10-core Intel Xeon E5-2690 v2 CPUs at 3.0 GHz and 255 GB RAM. Each virtual machine had three logical processing units and 20 GB RAM assigned.

A. Investigated methods

The assembly task is executed with two, three, and four robots. Each scheduling method was given 24 hours per experiment to optimize the assembly duration of each task. Five experiments per scheduling method were executed. The gradient-free optimization methods described in Section IV-B (SA, PSO and EA) were executed each with a random initialization, indicated by the keyword "Rand", and with an initialization with the sampling heuristic presented in Section IV-A, indicated by the keyword "Init". Similarly, MCTS and MCTS-G were each executed using the sampling heuristic as playout strategy for heavy playouts, random light playouts and mixed playouts. The percentage of random light playouts used is indicated so that, for example, "MCTS-G 10%" corresponds to MCTS-G with 10% light playouts and 90% heavy playouts. All scheduling methods are additionally compared to continuously sampling random schedules as a baseline.

B. Parameters

The maximum assembly duration was set to $d_{\max} = 40$ seconds. All scheduling methods used a time discretization of 0.2 seconds, resulting in 200 time steps. The specific parameters of the presented methods that were used in the experiment are presented below.

1) *Parameters of the sampling heuristic:* The main parameter of the sampling heuristic introduced in Section IV-A is the probability distribution for selecting start time steps. The selection probability p of a time step $t_i \in I = [t_0, \dots, t_M]$ is determined using a function $f : \mathbb{R} \rightarrow \mathbb{R}$:

$$p(t_i) = \frac{f(t_i - t_0)}{\sum_{j=0}^M f(t_j - t_0)}$$

A quadratically declining probability distribution is implemented using a function f_q :

$$f_q(x) = \frac{1}{(x + 2)^2} \quad (8)$$

2) *Parameters of the gradient-free optimization methods:* The parameters of the statistical cooling strategy of the SA algorithm are as follows:

$$\begin{aligned} x_0 &= 0.95, & \delta &= 0.2 \\ m_0 &= L = 20 \end{aligned}$$

Here, x_0 denotes the initial acceptance rate, δ governs the temperature update, L is the number of transitions for each temperature update, and m_0 is the number of transitions used to determine the initial temperature. A detailed description of the algorithm is given in [19].

In PSO, a single particle's velocity update is given by:

$$v_{i+1}^p = w^p v_i^p + c_{\text{soc}} \epsilon_1 (x_{\text{best}}^g - x_i^p) + c_{\text{cog}} \epsilon_2 (x_{\text{best}}^p - x_i^p)$$

With w^p denoting the inertia, c_{soc} is the social weight, c_{cog} is the cognitive weight, x_{best}^g is the global best solution, x_{best}^p is the particle's individual best solution and ϵ_1 and ϵ_2 are random numbers in the range $[0, 1]$. This update was suggested by [30]. The values of the parameters are:

$$\begin{aligned} w^p &= 0.9, & c_{\text{soc}} &= 2, & c_{\text{cog}} &= 1 \\ N_p &= 15, & v_{\min} &= -20, & v_{\max} &= 20 \end{aligned}$$

The variable N_p is the number of particles and v_{\min} and v_{\max} are bounds on the randomly chosen initial velocity.

The EA holds a population of $N_{\text{EA}} = 15$ individuals. Recombination is achieved by n -point crossover with $n = 5$ crossover points. The seven best individuals in each iteration are recombined until 14 descendants are created. They are mutated by randomly selecting 20% of their values and changing them to values sampled from a normal distribution around the original value and standard deviation $\sigma = 3$. The best individual of each iteration is transferred to the next iteration as the 15th descendant.

The objective function in (6) is extended as described in Section V-D and the weights are set to:

$$\mu_1 = 30, \quad \mu_2 = 900, \quad \mu_3 = 10, \quad \mu_4 = 1$$

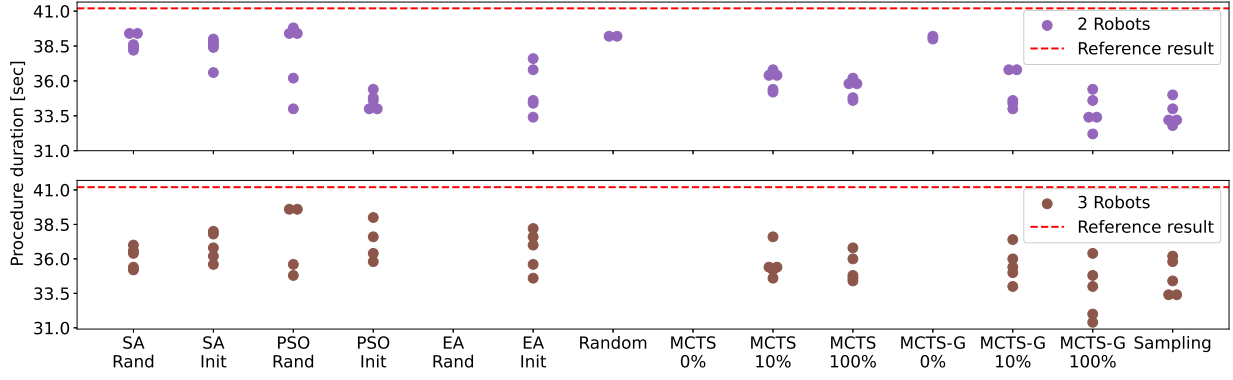


Fig. 8. Optimized solutions after five experiments.

3) *Parameters of the MCTS variants:* For both MCTS variants, the weights in the result value function are:

$$\lambda_1 = 0.01, \quad \lambda_2 = 1, \quad \lambda_3 = 0.1$$

and the parameter c for the UCT selection policy is $c = \sqrt{2}$. For MCTS-G, the selection termination probability at a leaf node with at least one explored child node is set to 10%.

4) *Parameters of the motion planning:* For the experiments, the limit of sampling attempts without finding a collision-free sample on each section border was set to $L_0 = 10$. The time limit for the path planning algorithms was set to $T_{max} = 30 \times n_r$ seconds, and the time limit for advancing the guide path was set to 15 minutes.

C. Results

First, the sampling heuristic with the described parameters was investigated. A quadratically declining probability distribution was found to strike a good balance between providing good solutions and being able to find diverse solutions to many problems.

Figure 8 shows the optimized solutions of all investigated methods in structural configurations with two and three robots. For the sampling heuristic, this corresponds to the best found solution of each experiment. "Random" indicates randomly generated schedules and "Sampling" indicates the sampling heuristic with a quadratically declining probability distribution.

Observing the optimized solutions, random schedules, MCTS and MCTS-G with purely light playouts, and EA with random initialization were not able to find a solution in all experiments. Neither in structural configurations with two robots nor with three robots. A clearly best performing method over all experiments cannot be determined with the data.

To verify the applicability of the general method to structural configurations with four robots as well, PSO with initialization using the sampling heuristic, MCTS-G with purely heavy playouts, and the sampling heuristic with a quadratically declining probability distribution were applied. Figure 9 shows the found optimized solutions in a structural configuration with four robots. Each of the selected methods was able to reliably solve the assembly task.

The solution approach can be compared to the procedure gen-

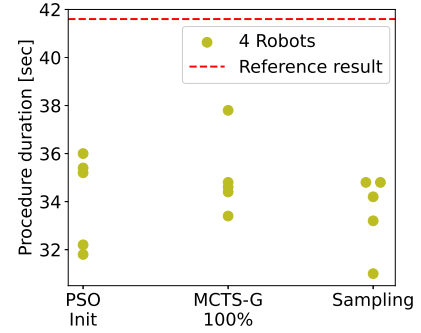


Fig. 9. Optimized solutions in a structural configuration with four robots after five experiments.

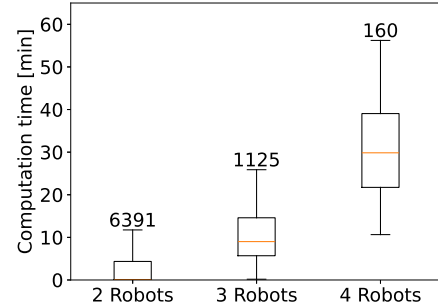


Fig. 10. Computation time for successful motion planning.

eration approach presented in [15] by comparing the optimized solution for the same assembly task and the same process operation assignment. Applying the method of [15] with a fixed process operation assignment yields assembly durations of 41.2 seconds for structural configurations with two and three robots and 41.6 seconds for the structural configurations with four robots. This reference result is illustrated as a red dashed line in Figure 8 and Figure 9. A reduction of the assembly duration by 10% to 20% can be expected.

The computation time for successful motion planning in structural configurations with two, three, and four robots is illustrated in Figure 10. The visualization as boxplots shows the median as an orange line, a box containing 50% of the

solutions and whiskers containing 90% of the solutions. The number above each boxplot indicates the number of data points considered for each boxplot. Figure 10 suggests a non-linear increase in computation time with the number of robots.

VII. CONCLUSION AND LIMITATIONS

This paper presents an approach for minimizing the assembly duration in reconfigurable multi-robot assembly cells, assuming a fixed structural configuration and a fixed assignment of assembly steps to the robots. Assembly steps are segmented into core operations, which are process-defining and pre-planned, and traverse operations, which connect these. The temporal scheduling of core operations is optimized using three different strategies: a sampling-based heuristic, a decision tree, and different gradient-free optimization methods. To exploit optimization potential in the traverse operations, a semi-centralized multi-robot motion planning method is introduced. It identifies *problem areas*, segments of the task where decentralized motion planning is insufficient, and subdivides them into *sections* of constant C -space dimensionality and constant modes of the involved robots. A cross-sectional roadmap is constructed for each *problem area* and used to determine *guide paths* which serve as skeletons for full solution paths. These skeletons are refined using standard motion planners. When planning fails, the magnitude of failure is expressed and fed back into the scheduling method which can then adapt the schedule accordingly.

The results show that the presented approach successfully reduces the assembly duration compared to existing methods by finding coordinated motions for multiple robots. The general definition of core operations allows the approach to be applied to a wide variety of assembly tasks, provided that each core operation has a known duration and known collision geometry over time.

One limitation is the pre-planning and fixation of core operation motions, which restricts optimization potential. Different motion variants for core operations could result in more efficient traverse operations and a shorter overall assembly duration. More complete approaches, such as the one by [14], can exploit multiple motion variants for core operations and potentially achieve better results.

The scheduling problem formulation allows for the use of various optimization approaches. This work explores six different methods. No single method emerged as clearly superior, indicating that further exploration is needed.

While the computation time is generally adequate for adaptive assembly systems, the methods are not fast enough to be used in higher-level iterative optimizations of structural configurations or assembly step assignments. Additionally, the computation time does not scale linearly with the number of robots used.

The motion planning results are geometric paths in the X -space of the corresponding robots. Although velocity and acceleration constraints are partially considered, the timed geometric paths are not directly executable in real systems. This limitation stems from linear interpolation between joint configurations and the decomposition into independently solved

subproblems. While smoothing techniques such as short-cutting and moving-average smoothing are applied, further post-processing is required to generate dynamically feasible trajectories that maintain timing and avoid collisions. This may not be possible for all traverse operations and could render the found solutions inapplicable, motivating future work.

Finally, integrating this approach into a holistic optimization framework that considers both the structural and procedural configuration of reconfigurable multi-robot assembly cells is a promising direction for future research.

REFERENCES

- [1] H. A. ElMaraghy and H.-P. Wiendahl, *Changeable and Reconfigurable Manufacturing Systems*, H. A. ElMaraghy, Ed. Springer London, 2009.
- [2] K. Kant and S. W. Zucker, "Toward efficient trajectory planning: The path-velocity decomposition," *The International Journal of Robotics Research*, vol. 5, no. 3, pp. 72–89, 1986.
- [3] H. Pham and Q.-C. Pham, "A new approach to time-optimal path parameterization based on reachability analysis," *IEEE Transactions on Robotics*, vol. 34, no. 3, pp. 645–659, 2018.
- [4] A. Sintov and A. Shapiro, "Time-based RRT algorithm for rendezvous planning of two dynamic systems," in *2014 IEEE International Conference on Robotics and Automation (ICRA)*. Hong Kong, China: IEEE, June 2014, pp. 6745–6750.
- [5] F. Grothe, V. N. Hartmann, A. Orthey, and M. Toussaint, "St-rrt*: Asymptotically-optimal bidirectional motion planning through space-time," in *2022 International Conference on Robotics and Automation (ICRA)*, Philadelphia, PA, USA, May 2022, pp. 3314–3320.
- [6] M. Erdmann and T. Lozano-Perez, "On multiple moving objects," *Algorithmica*, vol. 2, pp. 477 – 521, January 1987.
- [7] A. Shkolnik and R. Tedrake, "Path planning in 1000+ dimensions using a task-space voronoi bias," in *2009 IEEE International Conference on Robotics and Automation (ICRA)*. Kobe, Japan: IEEE, May 2009, pp. 2061–2067.
- [8] A. Orthey, S. Akbar, and M. Toussaint, "Multilevel motion planning: A fiber bundle formulation," *The International Journal of Robotics Research*, vol. 43, no. 1, pp. 3–33, 2024.
- [9] J. van den Berg, J. Snoeyink, M. Lin, and D. Manocha, "Centralized path planning for multiple robots: Optimal decoupling into sequential plans," in *Proceedings of Robotics: Science and Systems*, Seattle, USA, 2009.
- [10] K. Hauser and J.-C. Latombe, "Multi-modal motion planning in non-expansive spaces," *International Journal of Robotics Research*, vol. 29, pp. 897 – 915, 2010.
- [11] K. Hauser and V. Ng-Thow-Hing, "Randomized multi-modal motion planning for a humanoid robot manipulation task," *The International Journal of Robotics Research*, vol. 30, no. 6, pp. 678–698, 2011.
- [12] C. R. Garrett, R. Chitnis, R. Holladay, B. Kim, T. Silver, L. P. Kaelbling, and T. Lozano-Pérez, "Integrated task and motion planning," *Annual Review of Control, Robotics, and Autonomous Systems*, vol. 4, no. 1, pp. 265–293, 2021.
- [13] V. N. Hartmann, A. Orthey, D. Driess, O. S. Oguz, and M. Toussaint, "Long-horizon multi-robot rearrangement planning for construction assembly," *IEEE Transactions on Robotics*, vol. 39, no. 1, pp. 239–252, 2023.
- [14] J. Chen, J. Li, Y. Huang, C. Garrett, D. Sun, C. Fan, A. Hofmann, C. Mueller, S. Koenig, and B. C. Williams, "Cooperative task and motion planning for multi-arm assembly systems," arXiv preprint arXiv:2203.02475, 2022.
- [15] M. Ungen, E. Huber, D. Kampert, and O. Riedel, "Assembly procedure generation for reconfigurable robot cells considering operation concurrency and geometrical constraints," in *2024 IEEE 20th International Conference on Automation Science and Engineering (CASE)*, Bari, Italy, September 2024, pp. 981–987.
- [16] H. Zhang, S.-H. Chan, J. Zhong, J. Li, P. Kolapo, S. Koenig, Z. Agioutantis, S. Schafrik, and S. Nikolaidis, "Multi-robot geometric task-and-motion planning for collaborative manipulation tasks," *Autonomous Robots*, vol. 47, no. 8, pp. 1537–1558, 2023.
- [17] D. Mateu-Gomez, F. J. Martínez-Peral, and C. Perez-Vidal, "Multi-arm trajectory planning for optimal collision-free pick-and-place operations," *Technologies*, vol. 12, no. 1, p. 12, 2024.
- [18] S. Kirkpatrick, C. D. Gelatt, and M. P. Vecchi, "Optimization by simulated annealing," *Science*, vol. 220, no. 4598, pp. 671–680, 1983.

- [19] E. H. L. Aarts and P. J. M. Van Laarhoven, "Statistical cooling: A general approach to combinatorial optimization problems," *Philips Journal of Research*, vol. 40, no. 4, pp. 193–226, 1985.
- [20] K. Döring and H. Gordon Petersen, "Multi-robot task scheduling in micro-manufacturing," in *The 6th IEEE International Symposium on Assembly and Task Planning: From Nano to Macro Assembly and Manufacturing (ISATP)*. Montreal, Quebec, Canada: IEEE, July 2005, pp. 125–131.
- [21] R. Eberhart and J. Kennedy, "A new optimizer using particle swarm theory," in *MHS'95. Proceedings of the Sixth International Symposium on Micro Machine and Human Science*, Nagoya, Japan, October 1995, pp. 39–43.
- [22] L. Kocsis and C. Szepesvári, "Bandit based monte-carlo planning," in *Proceedings of the 17th European Conference on Machine Learning*, Berlin, Germany, September 2006, pp. 282–293.
- [23] E. W. Dijkstra, "A note on two problems in connexion with graphs," *Numerische Mathematik*, vol. 1, no. 1, pp. 269–271, 1959.
- [24] L. Kavraki, P. Svestka, J.-C. Latombe, and M. Overmars, "Probabilistic roadmaps for path planning in high-dimensional configuration spaces," *IEEE Transactions on Robotics and Automation*, vol. 12, no. 4, pp. 566–580, 1996.
- [25] J. Kuffner and S. LaValle, "Rrt-connect: An efficient approach to single-query path planning," in *Proceedings 2000 ICRA. Millennium Conference. IEEE International Conference on Robotics and Automation.*, San Francisco, CA, USA, April 2000, pp. 995–1001.
- [26] P. Chen and Y. Hwang, "SANDROS: a dynamic graph search algorithm for motion planning," *IEEE Transactions on Robotics and Automation*, vol. 14, no. 3, pp. 390–403, 1998.
- [27] R. Geraerts and M. H. Overmars, "Creating high-quality paths for motion planning," *The International Journal of Robotics Research*, vol. 26, no. 8, pp. 845–863, 2007.
- [28] E. Coumans and Y. Bai, "Pybullet, a python module for physics simulation for games, robotics and machine learning," <http://pybullet.org>, 2016–2023.
- [29] I. A. Şucan, M. Moll, and L. E. Kavraki, "The Open Motion Planning Library," *IEEE Robotics & Automation Magazine*, vol. 19, no. 4, pp. 72–82, December 2012, <https://ompl.kavrakilab.org>.
- [30] Y. Shi and R. Eberhart, "A modified particle swarm optimizer," in *1998 IEEE International Conference on Evolutionary Computation Proceedings. IEEE World Congress on Computational Intelligence*, Anchorage, AK, USA, May 1998, pp. 69–73.



Elias Huber is a researcher at Bosch Corporate Research, focusing on simulation-based planning approaches for reconfigurable robot cells. He received his B.Sc. and M.Sc. in Mechanical Engineering from Karlsruhe Institute of Technology (KIT), Germany. Currently, he is pursuing a Ph.D. at the Institute for Material Handling and Logistics (IFL) at KIT.



Jan-Felix Klein is currently a postdoctoral researcher at the Institute for Material Handling and Logistics (IFL) at the Karlsruhe Institute of Technology (KIT), Germany, where he received his Dr.-Ing. degree. His research focusing on automation and robotics applied in intralogistics with a special focus on circular production. He received a B.Sc. and M.Sc. in Industrial Engineering from the University of Duisburg-Essen.



Loris Schneider received his B.Sc. and M.Sc. in Mechatronics and Information Technology from Karlsruhe Institute of Technology (KIT), Germany. He is currently a Ph.D. student at the Institute for Material Handling and Logistics (IFL) at KIT, focusing on Artificial Intelligence and Robotics.



Marc Ungen is a researcher at Bosch Corporate Research, focusing on simulation-based planning approaches for reconfigurable robot cells. He holds a B.Eng. in Mechanical Engineering and an M.Sc./M.Eng. in Industrial Engineering. Currently, he is pursuing a Ph.D. at the Institute for Control Engineering of Machine Tools and Manufacturing Units (ISW), University of Stuttgart, Germany.